

RICE UNIVERSITY

Heat Transfer of a Single Wall Carbon Nanotube

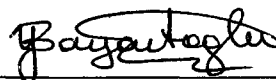
by

Robert A. Shelley


A THESIS SUBMITTED
IN PARTIAL FULFILLMENT OF THE
REQUIREMENTS FOR THE DEGREE

Master of Science

APPROVED, THESIS COMMITTEE:



Yildiz Bayazitoglu, Chair
H. S. Cameron Chair Professor in
Mechanical Engineering



Andrew J. Meade
Professor of Mechanical Engineering and
Material Science



Boris I. Yakobson
Professor of Mechanical Engineering and
Material Science
Professor of Chemistry

Houston, Texas

May, 2009

UMI Number: 1466840

INFORMATION TO USERS

The quality of this reproduction is dependent upon the quality of the copy submitted. Broken or indistinct print, colored or poor quality illustrations and photographs, print bleed-through, substandard margins, and improper alignment can adversely affect reproduction.

In the unlikely event that the author did not send a complete manuscript and there are missing pages, these will be noted. Also, if unauthorized copyright material had to be removed, a note will indicate the deletion.

UMI[®]

UMI Microform 1466840
Copyright 2009 by ProQuest LLC
All rights reserved. This microform edition is protected against
unauthorized copying under Title 17, United States Code.

ProQuest LLC
789 East Eisenhower Parkway
P.O. Box 1346
Ann Arbor, MI 48106-1346

ABSTRACT

Heat Transfer of a Single Wall Carbon Nanotube

by

Robert A. Shelley

A non equilibrium molecular dynamics simulation was used to calculate thermal conductivity of a single-walled carbon nanotube (SWNT). Effective thermal conductivity was calculated for the same SWNT surrounded by nitrogen at 250K and 290K at 8 bar. Heat flux was created by implementing Nose-Hoover thermostats at the ends of the SWNT. Using Fourier's Law thermal conductivity was calculated. For both simulations thermal conductivity increased when the temperature difference between the two ends was small. As the temperature difference increased the thermal conductivity reached a constant value of around 160 W/mK in a vacuum with end temperatures close to 330K or 310K.

Acknowledgments

This work was supported in part by the financial contribution of the Mechanical Engineering and Materials Science Department at Rice University, LANCER Grant from the Lockheed Inc, the Shared University Grid at Rice funded by NSF under Grant EIA-0216467, and a partnership between Rice University, Sun Microsystems, and Sigma Solutions, Inc. I would also like to thank J.T. Frey for sending the "Tubegen" code.

Contents

| | |
|--|-----------|
| Abstract | ii |
| Acknowledgments | iii |
| List of Illustrations | vi |
| List of Tables | viii |
| 1 Introduction | 1 |
| 1.1 Single Wall Carbon Nanotubes | 1 |
| 1.1.1 Structure | 1 |
| 1.1.2 Properties | 2 |
| 1.1.3 Nanocarpets | 2 |
| 1.2 Motivation and Objectives | 4 |
| 2 Molecular Dynamics | 7 |
| 2.1 Introduction | 7 |
| 2.2 Lennard-Jones Potential | 7 |
| 2.3 Dimensionless Units | 8 |
| 2.4 Periodic Boundary Conditions | 9 |
| 2.5 Berendsen Thermostat | 10 |
| 3 Thermal Conductivity | 12 |
| 3.0.1 Introduction | 12 |
| 3.0.2 Analysis | 12 |
| 3.0.3 Simulation Parameters | 13 |
| 3.0.4 Thermal Conductivity Calculation | 14 |

| | |
|--|----|
| 3.0.5 Thermal Conductivity in Vacuum | 19 |
| 3.0.6 Effective Thermal Conductivity | 23 |

| | |
|---------------------|-----------|
| 4 Conclusion | 30 |
|---------------------|-----------|

| | |
|---------------------|-----------|
| Bibliography | 32 |
|---------------------|-----------|

Illustrations

| | | |
|-----|--|----|
| 1.1 | Hexagonal lattice of a single wall carbon nanotube showing chiral and translational vectors [1] | 3 |
| 1.2 | Armchair, Zigzag, and Chiral nanotubes [2] | 4 |
| 1.3 | Schematic of Nanocarpets | 5 |
| 2.1 | Periodic boundary conditions in 2-D | 10 |
| 3.1 | Schematic of SWCNT with set ends being of length $2L_c$ | 14 |
| 3.2 | Axial temperature profile of a SWNT (5,5) with the base temperature at 310 K at $x=0$ nm and 290 K at $x=12.3$ nm and heated base lengths of 12.3nm and 24.6nm. | 17 |
| 3.3 | Axial temperature profile of a SWNT (5,5) with the base temperature at 310 K at $x=0$ nm and 290 K at $x=12.3$ nm and heated base lengths of 6.15nm | 18 |
| 3.4 | Axial temperature profile of a SWNT (5,5) with the base temperature at 310 K at $x=0$ nm and various temperatures at $x=12.3$ nm with a heated base lengths of 24.6nm. | 20 |
| 3.5 | Axial temperature profile of a SWNT (5,5) with the base temperature at 330 K at $x=0$ nm and various temperatures at $x=12.3$ nm with a heated base lengths of 24.6nm. | 21 |

| | | |
|------|--|----|
| 3.6 | Axial temperature profile of a SWNT (5,5) with the base temperature at 290 K at $x=0$ nm and various temperatures at $x=12.3$ nm with a heated base lengths of 24.6nm. | 22 |
| 3.7 | Thermal conductivity compared for average temperature, $\frac{T_{l1}+T_{l2}}{2}$, of SWNT with T_a at 330K and 310K | 24 |
| 3.8 | Thermal conductivity compared change in temperature of linear part, $T_{l1} - T_{l2}$, of axial temperature profile T_a at 330K and 310K | 25 |
| 3.9 | Axial temperature profile of a SWNT (5,5) with the base temperature at 310 K at $x=0$ nm and various temperatures at $x=12.3$ nm with a heated base lengths of 24.6nm and surrounding nitrogen at 250K. The axial temperature profiles for a vacuum under the same conditions are plotted with the dotted line with out markers. | 26 |
| 3.10 | Axial temperature profile of a SWNT (5,5) with the base temperature at 310 K at $x=0$ nm and various temperatures at $x=12.3$ nm with a heated base lengths of 24.6nm and surrounding fluid at 290K. The axial temperature profiles for a vacuum under the same conditions are plotted with the dotted line with out markers. | 27 |
| 3.11 | Effective thermal conductivity compared with $T_a = 310K$ and T_b varies with nitrogen at 250K and 290K overlaid with results for thermal conductivity in a vacuum. | 28 |

Tables

| | |
|--|----|
| 3.1 Lennard-Jones parameters | 14 |
|--|----|

Chapter 1

Introduction

Sumio Iijima in 1991 discovered what is today termed single wall carbon nanotubes (SWNTs)[3]. The science community for almost two decades has been studying, understanding, and apply the amazing mechanical, thermal and electrical properties of these tubes[4][5].

Current trends in reducing the size of electronics and running smaller more efficient reactions has created a demand for increased heat transfer on the microscopic level. Microchannels have been implemented to help increase the heat transfer of these small devices, but higher heat transfer is still needed. Due to SWNTs high thermal conductivity arrays have been considered to improve heat transfer properties.

In this research Molecular Dynamics (MD) is used to further understand heat transfer of a SWNT. Understanding limiting effects in MD will allow more efficient arrays to be implemented. These advances could then be implemented into the packaging of smaller more efficient devices.

1.1 Single Wall Carbon Nanotubes

1.1.1 Structure

A carbon nanotube can be described as a graphene sheet rolled up to create a seamless tube. The diameter of the nanotube can be as large as 30 nm with a length in the microns [3].

A given tube is defined based up on the vector, C_h , and translational vector, T , defined in the hexagonal lattice shown in Figure 1.1 and by Equation 1.1.

$$C_h = na_1 + ma_2 \quad (1.1)$$

The properties of a SWNT are defined by the index number of the chiral vectors n and m in Equation 1.1 and can be described by three main categories zigzag, armchair, and chiral. Zigzag is defined if $m = 0$ shown in the middle of Figure 1.2. If $n = m$ then it is called an armchair shown in in the at the top of Figure 1.2. Other defined chiral vectors are called chiral shown at the bottom of Figure 1.2.

The axis of the nanotube is defined by the translational vector, T , and is normal to the chiral vector, C_h , in Figure 1.1.

In summary a SWNT can be defined by the translational vector, T , and the chiral vector, C_h . The translational vector defines the axis of the tube while the chiral vector defines the diameter and chirality of the SWNT.

1.1.2 Properties

The electrical property of a perfect SWNT is defined by the chirality. Metallic properties exist when $n - m$ is divisible by a factor of 3. Therefore all armchair SWNT have metallic properties. All other chiralites define a nanotube with semi-conductor properties. Defects in the SWNT will make this rule become invalid.

1.1.3 Nanocarpet

A nanocarpet is an array of SWNTs aligned vertically used to increase heat transfer removal similar to an array of pins fin used to increase heat transfer from an extended surface on the macroscopic level. Given the limitations of fluid velocity at the microscopic level and the general impracticality of decreasing the temperature of the gas

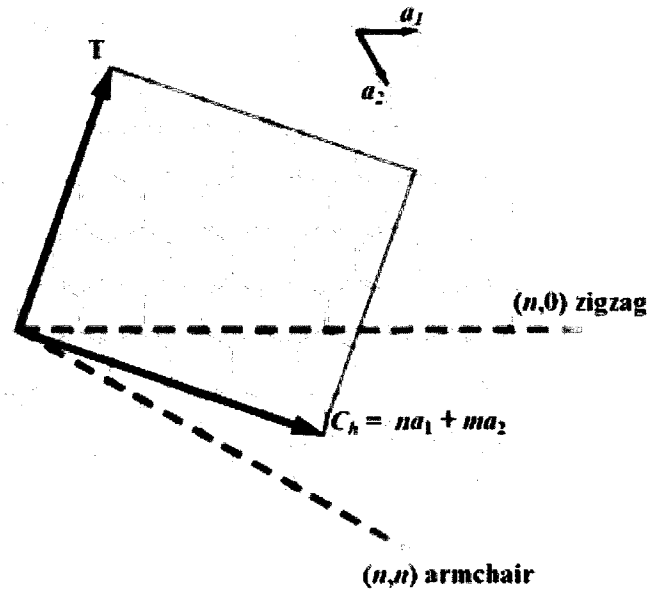


Figure 1.1 : Hexagonal lattice of a single wall carbon nanotube showing chiral and translational vectors [1]

increasing the surface area with SWNT would effectively increase the heat transfer. The area is increased by extending the surface area from the wall into the moving medium. To improve the heat transfer the fins should have high thermal conductivity to not create additional resistance for the energy moving away from the system. The fin itself creates conduction resistance with the base not guaranteeing an increase in heat transfer. The fin spacing could also limit flow as a result of blocking [6] fluid flow. Figure 1.3 shows an approach to investigate a medium flowing above and into the array of fins. Not a fin being as long or as wide as the cross sectional area of the channel as it is in [6].

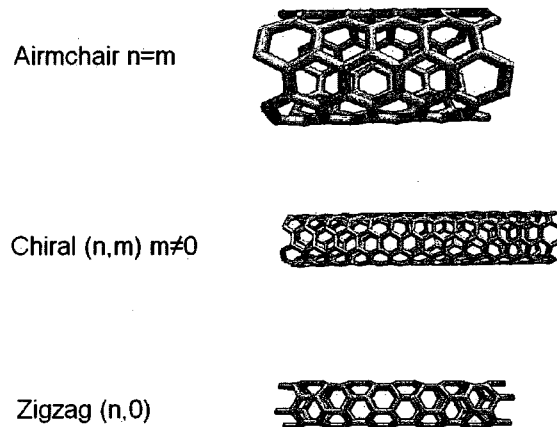


Figure 1.2 : Armchair, Zigzag, and Chiral nanotubes [2]

1.2 Motivation and Objectives

In the past it has been predicted that single phase microchannel forced convective cooling could handle $1,000 \text{ W/cm}^2$ loads [7]. Current design road maps suggest that 8 nm electronic devices will produce even higher heat fluxes, $100,000 \text{ W/cm}^2$ [8] [9]. Effectively removing the thermal energy is a limiting factor in chip performance. Single wall carbon nanotubes (SWNTs) have been shown to reach thermal conductivity of $6,000 \text{ W/m}\cdot\text{K}$ [10] or multi walled carbon nanotubes (MWCNT) $3,000 \text{ W/m}\cdot\text{K}$ [11] [12]. Combining a microchannel with SWNT could effectively meet the thermal requirements needed for die designs. Current applications could extended to cooling of Micro-Electro-Mechanical Systems, reducing size of thermo voltaic cells, and improved efficiency in use of carbon nanotubes (CNTs) in solar water splitting. It has already been shown that laser patterned carbon nanotubes attached to chips can be a lightweight and effective cooling solution [13].

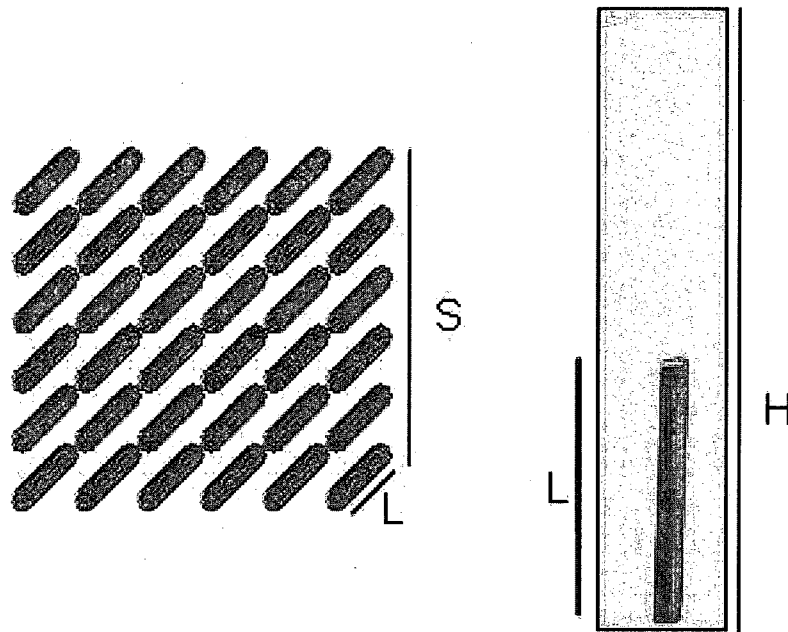


Figure 1.3 : Schematic of Nanocarpets

This thesis is focused on using molecular dynamics (MD) to analyze the thermal conductivity of a SWNT to lead to the analysis of a pin fin where the base of the nanotube is heated. Understanding one SWNT will give information into how arrays in a nanocarpets could behave. MD simulations of macro scale properties including heat transfer as a new direction from statistical mechanics and chemistry [14]. Radial conduction heat transfer MD simulation of a SWNT to air, where the heat source is axial inside the nanotube and heat sink is at a given radial distance from the center of the tube, have been analyzed in [15] by looking at how different pressures effect conduction to air and Kapitza length. Thermal boundary resistance of a CNT to octane liquid has also been simulated with MD [16]. Both studies showed the greatest thermal resistance is at the CNT liquid or air interface. Cases have been studied

in liquid suspensions [17] and polymer composites [18]. The static fluid creates an insulated layer around the tube. This thickness is called the Kapitza length, l_k :

$$l_k = \kappa U \quad (1.2)$$

where κ is the thermal conductivity and U the overall heat transfer. Fluid flow decreases the insulating layer and therefore shortens the Kapitza length.

The chirality used in the simulation has an impact on the conduction of the SWNT. Osman showed that at higher temperatures larger chiralities in armchair configuration had an increase in heat conduction. Overall SWNTs with metallic characteristic chiralities heat conduction did not depend on chirality, but more on diameter[19]. It was stated that the shift was due to radius dependent not chirality dependent umklapp scattering and heat transfer through radial phonons[20].

Non equilibrium molecular dynamics (NEMD) has been utilized in several examples to develop fluid flow ranging from uniform flow to shear flow[21][22][23]. Since an external force needs to be applied to the system to realize a flow, energy must be added to create the force preventing the use of a PVT and NVE ensembles MD. The flow can be realized by applying a force to the fluid molecules resulting in a pressure difference across the simulation box.

This research's objectives is to utilize the GROMACS [24] software package to simulate and analyze a SWNT thermal conductivity. This will be performed by holding the temperature of the bases surrounding fluid at a constant temperature using a thermostat to produce an axial temperature profile.

Chapter 2

Molecular Dynamics

2.1 Introduction

MD is a modeling tool used to simulate microscopic systems. It is simply performed by integrating Newton's Laws of motion over a period of time. As processing power has become more affordable in recent years MD has been implemented to more complex and challenging systems. The increased use of simulations has developed more standard methodologies making results have similar scientific value to experimental results. MD simulations can be applied to a variety of problems including fundamental studies, phase transitions, collective behavior, complex fluids, polymers, solids, biomolecules, and fluid dynamics [25].

2.2 Lennard-Jones Potential

Potentials are used to define the interaction of a pair of atoms. There are two main interatomic forces between two atoms attraction and repulsion. If two atoms are compressed against each other a repulsive force exists. As seen in solids and liquids if two atoms are separated an attractive force exists between the two atoms. The first term in Equation 2.1 dominates at close distances and gives value to repulsive force. At further distances the second term dominates and represents the attractive force or Van der Waals' force.

The Lennard-Jones (LJ) potential has been shown to be in good agreement with

experimental findings in Argon [26], and is the simplest way to represent this interaction for atoms i and j is defined by the Lennar-Jones potential where ϵ is the strength of the interaction and σ defines a length scale both dependent on the molecules simulated.

$$u(r_{ij}) = 4\epsilon \left[\left(\frac{\sigma}{r_{ij}} \right)^{12} - \left(\frac{\sigma}{r_{ij}} \right)^6 \right] \quad (2.1)$$

The force corresponding to the LJ potential is shown in Equation 2.2.

$$f = -\nabla u(r) \quad (2.2)$$

The interaction between atom j and i can then be represented by Equation 2.3 from combining Equation 2.1 and Equation 2.2.

$$f_{ij} = \left(\frac{48\epsilon}{\sigma^2} \right) \left[\left(\frac{\sigma}{r_{ij}} \right)^{14} - \frac{1}{2} \left(\frac{\sigma}{r_{ij}} \right)^8 \right] \quad (2.3)$$

The force atom i exerts on atom j can be expressed by Newton's third law $f_{ij} = -f_{ji}$ so each atom pair needs to be calculated only once. Using Equation 2.3 the acceleration of the particle is easy to calculate using Newton's second law, $F = ma$.

2.3 Dimensionless Units

Dimensionless units are introduced to allow normally small values to be close to unity and to simplify the equations of motion. Using dimensionless units also allows the model to be scaled to different problems with different length scales. Using σ , m , and

ϵ to be units of length, mass and energy respectively.

$$\textit{length} : r \rightarrow r\sigma \quad (2.4a)$$

$$\textit{energy} : e \rightarrow e\epsilon \quad (2.4b)$$

$$\textit{time} : t \rightarrow t\sqrt{m\sigma^2/\epsilon} \quad (2.4c)$$

$$\textit{pressure} : p \rightarrow p\sigma^3/\epsilon \quad (2.4d)$$

$$\textit{density} : \rho \rightarrow \rho\sigma^3/m \quad (2.4e)$$

2.4 Periodic Boundary Conditions

A simulation is a finite system used to represent the behavior of an infinite system. The simulation must take place in a container with walls to contain the atoms in the simulation region. In a macroscopic system with a very large number of atoms only a few atoms would interact with the wall, around $N_m^{2/3}$ where N_m is the number of atoms. When dealing with a microscopic system where $N_m = 1000$ around 500 atoms are adjacent to a wall [25].

Periodic boundary conditions are imposed to constrain the atoms but allow freedom of movement. Atoms are allowed to leave one side of the simulation and return on the corresponding other side creating a periodic image of itself seen in Figure 2.1. The MD software has to allow for the interaction of the atom within the cutoff length to other atoms on the other side as it passes across a boundary in both time equations and integrations of motion. To prevent cyclical effects from one atom coming back and affecting itself the simulation region needs to be at least twice the cutoff length[25].

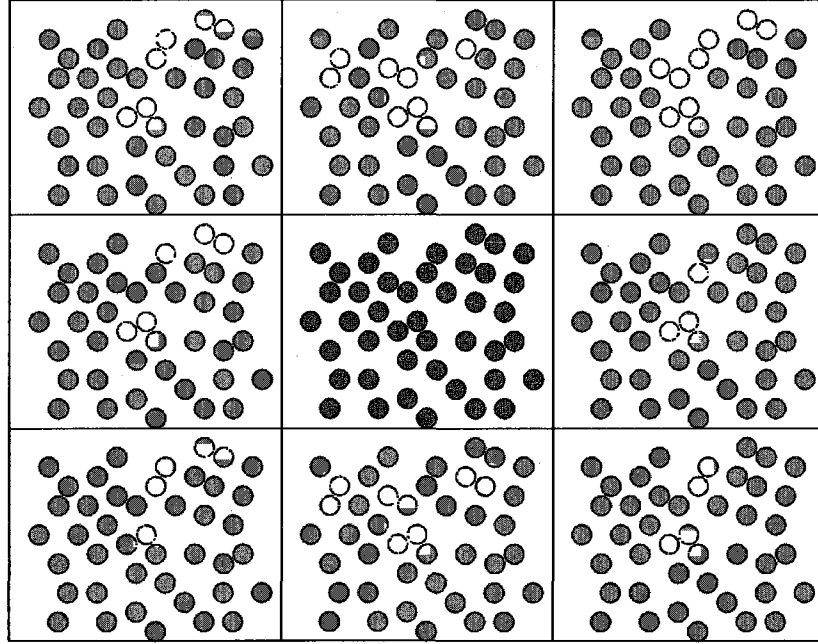


Figure 2.1 : Periodic boundary conditions in 2-D

2.5 Berendsen Thermostat

One method used to control the temperature of the simulation is to implement a velocity rescaling algorithm. The velocity rescaling is done by multiplying the velocities at each time step by λ .

$$\lambda = \sqrt{\frac{T_o}{T(t)}} \quad (2.5)$$

T_o is the set temperature and $T(t)$ is the temperature at a given time t calculated from the kinetic energy.

The Berendsen thermostat is similar to velocity rescaling but the rate of change in temperature is proportional to the temperature difference [27]. This replicates weak coupling to an external heat bath. Shown in the following where τ is the coupling

parameter, T_o is the set temperature, and $T(t)$ is the temperature calculated from kinetic energy at time t .

$$\frac{dT(t)}{dt} = \frac{1}{\tau}(T_o - T(t)) \quad (2.6)$$

The temperature difference decays exponentially over time with based upon the time constant, τ . The heat flow from scaling the velocities is represented as

$$\lambda^2 = 1 + \frac{\delta t}{\tau_T} \left\{ \frac{T_o}{T(t - \frac{\delta t}{2})} - 1 \right\}. \quad (2.7)$$

τ_T is close to τ but not exactly the same

$$\tau = 2C_v\tau_T/N_{df}k \quad (2.8)$$

where C_v is the total heat capacity of the system, k is the Boltzmann's constant, and N_{df} is the total number of degrees of freedom. $\tau \neq \tau_T$ because not all of the kinetic energy change goes directly into kinetic energy but some goes to potential energy.

Chapter 3

Thermal Conductivity

3.0.1 Introduction

The potential applications for a single wall carbon nanotubes (SWNT) has been growing since Iijima discovered them in 1991 [3]. Current processors require more efficient heat dissipation to increase chip speed. Single wall carbon nanotubes (SWNT) have shown high thermal conductivities even at short lengths and small chiralities[28] making them a good application in this environment. The SWNT's high thermal conductivities have been used in polymer composites to effectively increase heat transfer[29]. Keblinski studied the radial heat flux with the heat source and sink in the radial direction [15]. Therefore, creating a heat sink with SWNTs in array has the potential to efficiently increase heat flux.

The purpose of this study is to investigate the thermal conductivities of SWNT under different boundary conditions. This would allow the potential understanding of applications as a pin fin for cooling applications.

3.0.2 Analysis

An outline of the process implemented to determine the thermal conductivities of a SWNT are described in the following sections. The governing equations, parameters, and software will be discussed. All simulations were run on the Shared University Grid at Rice (SUG@R) running on 2 2.83Ghz Intel Xenon Quad Core processors with

16 GB of RAM per node.

3.0.3 Simulation Parameters

Harmonic potentials are used to model the bonded interactions of the C-C interactions within the SWNT using values from Guo[30], $k_{ij}^b = 478900 \text{ kJ/mol} \cdot \text{nm}^2$ and $b_{ij} = 0.14210 \text{ nm}$, in Equation 3.1. Harmonic potentials can be used since the length of the SWNT used is less than the mean free path of about 20 nm for a thermal conductivity of around 150 W/mK .

$$U(r_{ij}) = \frac{1}{2}k_{ij}^b(r_{ij} - b_{ij})^2 \quad (3.1)$$

Morse potentials are used to model the bonded interactions of O-O and N-N given by Equation 3.2

$$U(r_{ij}) = \epsilon_0[1 - e^{-k(r_{ij}-r_0)}]^2 \quad (3.2)$$

with $\epsilon_0 = 0.12070$ (0.1098) nm , $r_0 = 494.2105$ (941.692) kJ mol^{-1} , and $k = 0.2680$ (0.2642) nm^{-1} for O-O (N-N)[31]. Unbounded Intermolecular interactions are calculated with Lennard-Jones potentials.

$$U(r_{ij}) = 4\epsilon \left[\left(\frac{\sigma}{r_{ij}} \right)^{12} - \left(\frac{\sigma}{r_{ij}} \right)^6 \right] \quad (3.3)$$

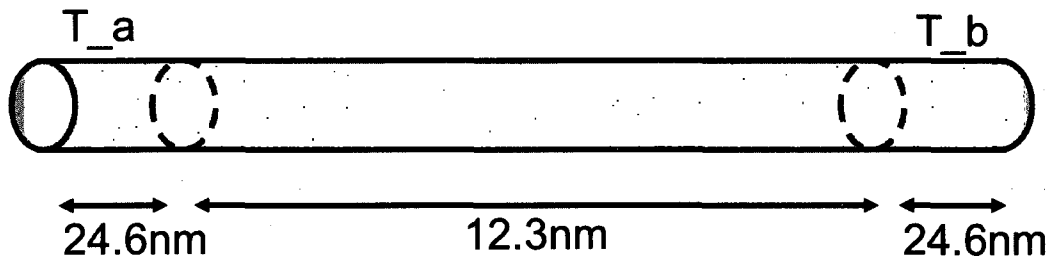
Parameters used are in Table 3.1 from the GROMOS forcefield in GROMACS[24] and additional parameters from literature[31].

Table 3.1 : Lennard-Jones parameters

| Pair | ϵ [kJ/mol] | σ [nm] |
|------|---------------------|--------------------------|
| C-C | 0.0023 | 0.33740×10^{-5} |
| C-N | 0.0042 | 7.9597×10^{-6} |
| C-O | 0.0038 | 5.7992×10^{-6} |
| N-N | 0.0076 | 1.8778×10^{-5} |
| O-O | 0.0061 | 9.9676×10^{-6} |
| O-N | 0.0069 | 1.6223×10^{-5} |

3.0.4 Thermal Conductivity Calculation

Thermal conductivity was calculated using non equilibrium molecular dynamics using an adapted procedure from Maruyama. Using the code called "Tubegen"[2] SWNTs with a length of 61.5 nm and 36.9 nm with a chirality of (5,5) were generated. Figure 3.1 shows a schematic of the simulation with the set end temperatures being twice the length of the section analyzed at corresponding to $2L_c$, where L_c is the length of the SWNT analyzed. The SWNT is placed in a vacuum and implements a Nose-

Figure 3.1 : Schematic of SWCNT with set ends being of length $2L_c$

Hoover thermostat, also used by Maruyama, to set the end temperatures, T_a and T_b , [28] to create heat flux along the SWNT. T_a was set to 330K, 310K, and 290K. T_b was then varied to look at how the thermal conductivity varied based upon the end temperatures. The magnitude of the equation of motion for a particle under the influence of a Nose-Hoover [32][33] thermostat can be represented as

$$\dot{p}_i = F_i - \xi p_i \quad (3.4)$$

and

$$\dot{\xi} = \frac{1}{Q}(T - T_0) \quad (3.5)$$

Where p is the magnitude of the momentum of atom i , F is the applied force on atom i , T_0 is the reference temperature, and T is the instantaneous temperature.

$$Q = \frac{\tau_T^2 T_0}{4\pi^2} \quad (3.6)$$

τ_T is the relaxation time and is set to 40 ps as done in Maruyama's work [34]. The heat transfer rate, J_i can be used to determine the heat flux using the momentum, p_i , and mass, m_i .

$$J_i = -\xi \frac{p_i \times p_i}{m_i} \quad (3.7)$$

The magnitude of the velocity of a particle at a given temperature, T , can be represented as

$$V = \sqrt{\frac{N_{df} k_b T}{m}} \quad (3.8)$$

where N_{df} is the number degrees of freedom, k_b is the Boltzmann constant, and m is the mass. Combining Equation 3.7 and Equation 3.8.

$$J = -\xi V^2 m_i \quad (3.9)$$

The heat flux per area would then be

$$q = \frac{J}{A} \quad (3.10)$$

Where $A = \pi b d$ and $b = 0.34 \text{ nm}$ based upon the Van der Waals thickness.

$$q = -k \frac{dT}{dx} \quad (3.11)$$

Using the slope of the linear section in Figure 3.2 with the calculated heat flux from Equation 3.10 to determine the thermal conductivity, k . A heated length of twice the original length shows that the slope of the line has converged between L_c and $2L_c$. Increasing the length of the section of SWNT controlled by the thermostat changes the heat flux along the tube. A length of twice the length being analyzed was determined to converge the heat flux. Changes in heat fluxes was also seen by Maruyama [28] by changing the length controlled by a thermostat, but their work did not use a value of heat flux that had converged. The temperature gradient was constant leaving only k to be a variable in Equation 3.11.

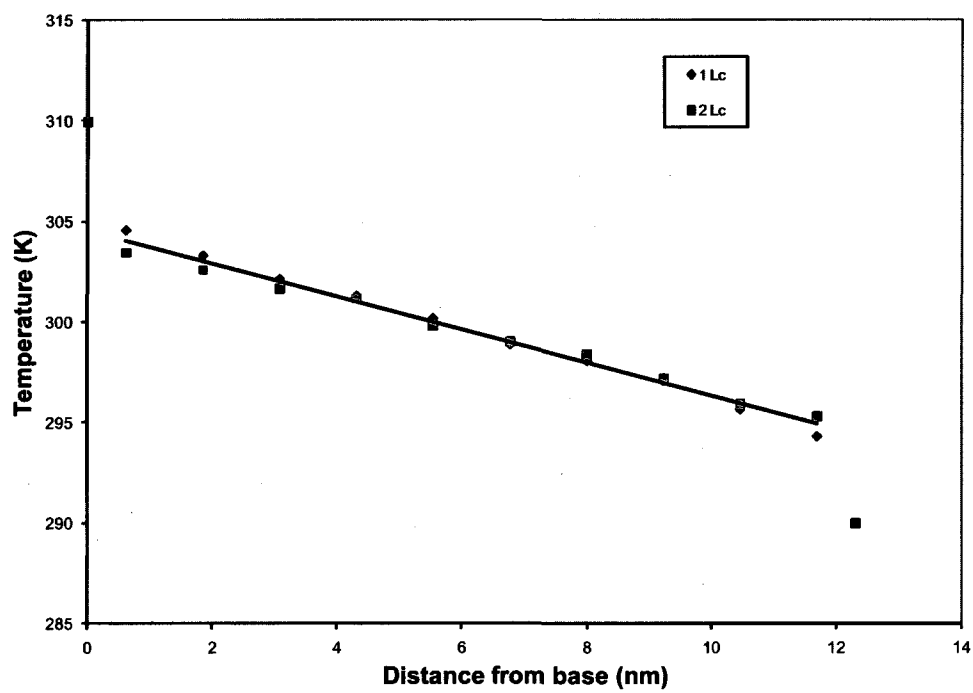


Figure 3.2 : Axial temperature profile of a SWNT (5,5) with the base temperature at 310 K at $x=0$ nm and 290 K at $x=12.3$ nm and heated base lengths of 12.3nm and 24.6nm.

Using a heat length of $0.5L_c$ resulted in the temperature profile seen in Figure 3.3. The thermal conductivity resulted in a value of $135 W/mK$ which is about the same value as Maruyama's results for a $12.3 nm$ long (5,5) SWNT[28]. This method used by Maruyama and adapted here has been shown to be in agreement with the Green-Kubo method[35]. Equation 3.12 represents how the thermal conductivity is calculated in measuring the equilibrium thermal conductivity.

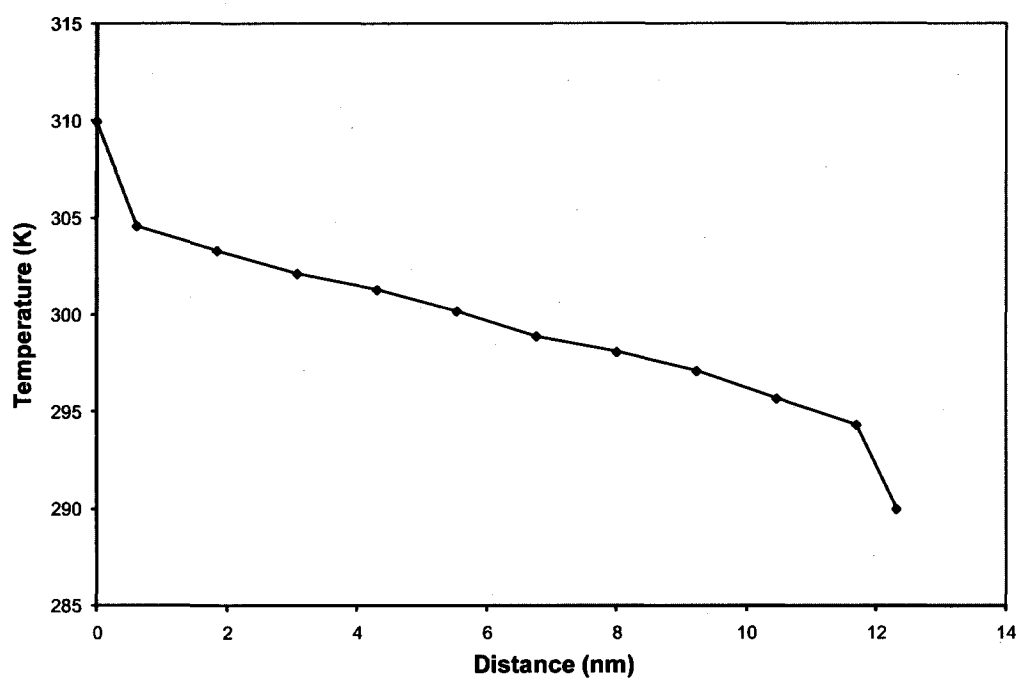


Figure 3.3 : Axial temperature profile of a SWNT (5,5) with the base temperature at 310 K at $x=0$ nm and 290 K at $x=12.3$ nm and heated base lengths of 6.15 nm

$$k = \frac{1}{k_b T^2 V} \int_0^\infty \langle J(t) \cdot J(0) \rangle dt \quad (3.12)$$

where

$$J(t) = \frac{d}{dt} \sum_i r_i(t) \epsilon_i(t) \quad (3.13)$$

and

$$\epsilon_i = \frac{1}{2} m_i v_i^2 + \frac{1}{2} \sum_j u(r_{ij}) \quad (3.14)$$

3.0.5 Thermal Conductivity in Vacuum

Each simulation was ran for $4 ns$, a time step of $0.5 fs$, and temperatures of each $1.23 nm$ section were time averaged for $2 ns$. The base section of $24.6 nm$ was heated using a Nose-Hoover thermostat with $\tau = 40 ps$ as shown in Figure 3.1.

Figure 3.4 shows various temperature profiles for $T_a = 310K$ and a range of temperatures for T_b in a vacuum. Diffusive heat transfer is seen at the ends and explained by the temperature jumps, while ballistic heat transfer is shown by the strong linear region in the middle. Similar trends were also seen in temperature profiles with $T_a = 330K$ in Figure 3.5 and $T_a = 290K$ in Figure 3.6. The diffusive temperature jumps were largest at the end fixed with a higher temperature.

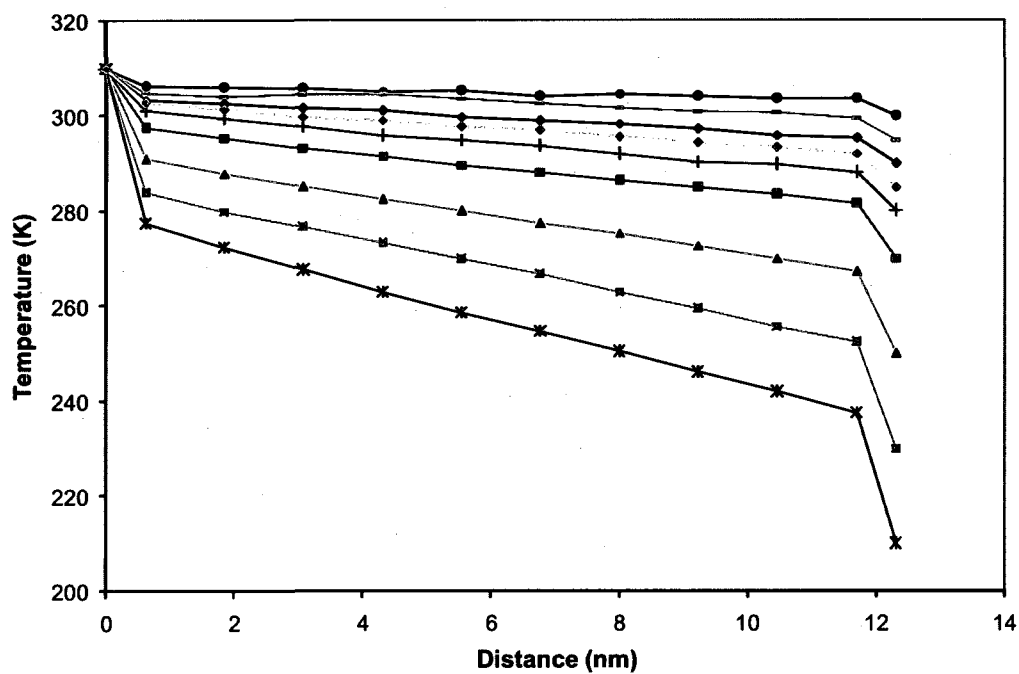


Figure 3.4 : Axial temperature profile of a SWNT (5,5) with the base temperature at 310 K at $x=0$ nm and various temperatures at $x=12.3$ nm with a heated base lengths of 24.6 nm.

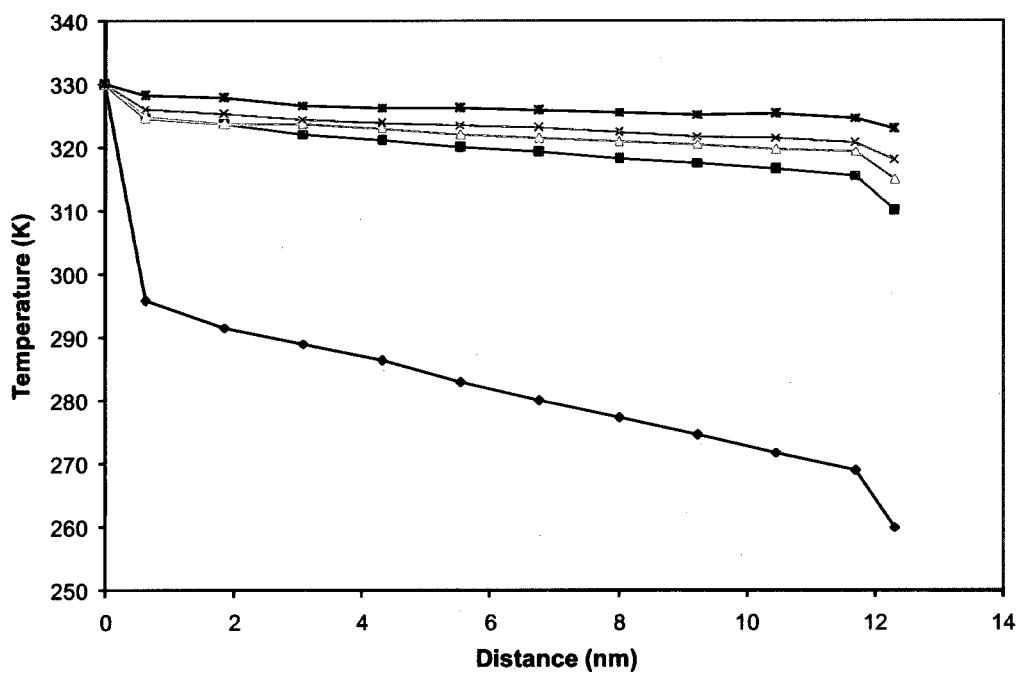


Figure 3.5 : Axial temperature profile of a SWNT (5,5) with the base temperature at 330 K at $x=0$ nm and various temperatures at $x=12.3$ nm with a heated base lengths of 24.6 nm.

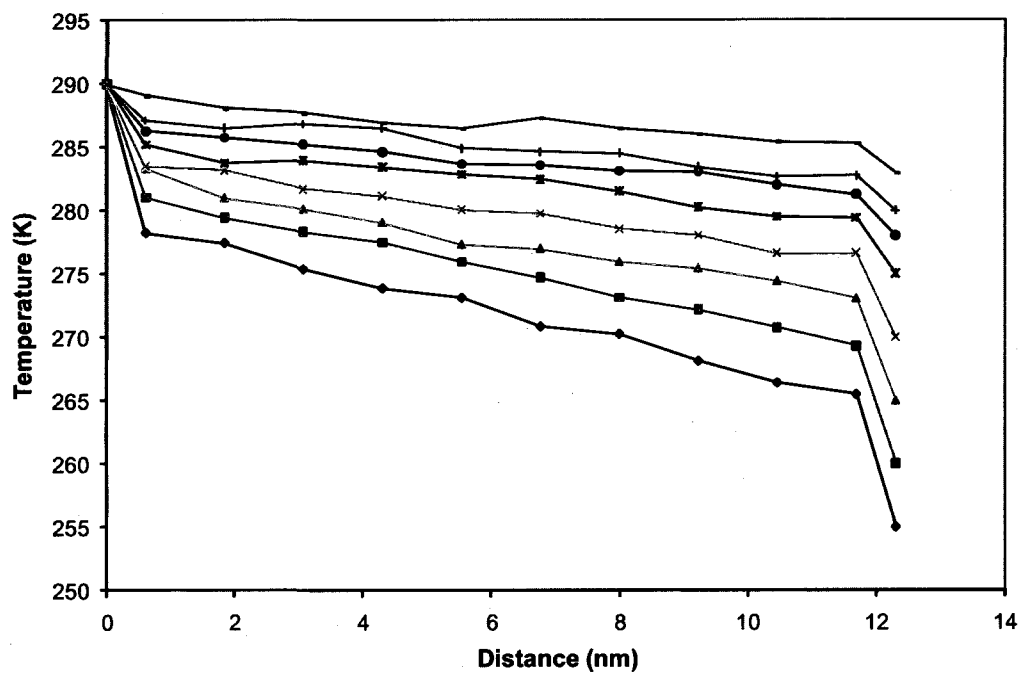


Figure 3.6 : Axial temperature profile of a SWNT (5,5) with the base temperature at 290 K at $x=0$ nm and various temperatures at $x=12.3$ nm with a heated base lengths of 24.6 nm.

Using the method described earlier the thermal conductivity was calculated for each change in temperature and is shown in Figure 3.7. Simulations for $T_a = 310K$ and $330K$ show as the average temperature of the linear region shown in Figure 3.4 approaches the temperature of T_a the thermal conductivity increase rapidly. The linear region can be described as the second data point from $x = 0nm$ as T_{l1} to the data point before $x = 12.3nm$ as T_{l2} . Reasoning for the increased the thermal conductivity could be explained similar to fluid flowing in a pipe. When the fluid flow or heat flux is small there is little resistance in transferring the fluid through the pipe, but when the pipe is full an increased resistance is seen limiting the rate that fluid can flow through the pipe with a constant pressure.

The same data was analyzed based upon the change in temperature of the linear region of the axial temperature profiles show in Figure 3.8. Thermal conductivity values for $T_a = 330K$ and $310K$ converged well for change in temperature of the linear regions as shown by the similar thermal conductivities at large temperature differences and a steep curve as the temperature differences become smaller.

3.0.6 Effective Thermal Conductivity

Simulations were then preformed using a SWNT surrounded by nitrogen to calculate an effective thermal conductivity at various nitrogen temperatures. The simulation box was $15.5\text{ nm} \times 15.5\text{ nm} \times 63.436\text{ nm}$ with 4000 nitrogen molecules held at a constant temperature of $290K$ or $250K$ using a Nose-Hoover thermostat with $\tau = 40ps$ resulting in a pressure of about 8 bar. The SWNT parameters were the same as used in Section 3.0.5. The simulations were ran for $2ns$ with the reported data being time averaged from $1 - 2ns$. Figures 3.9 and 3.10 show the axial temperature profiles. The profiles are not quite a linear as those seen in a vacuum. The effective

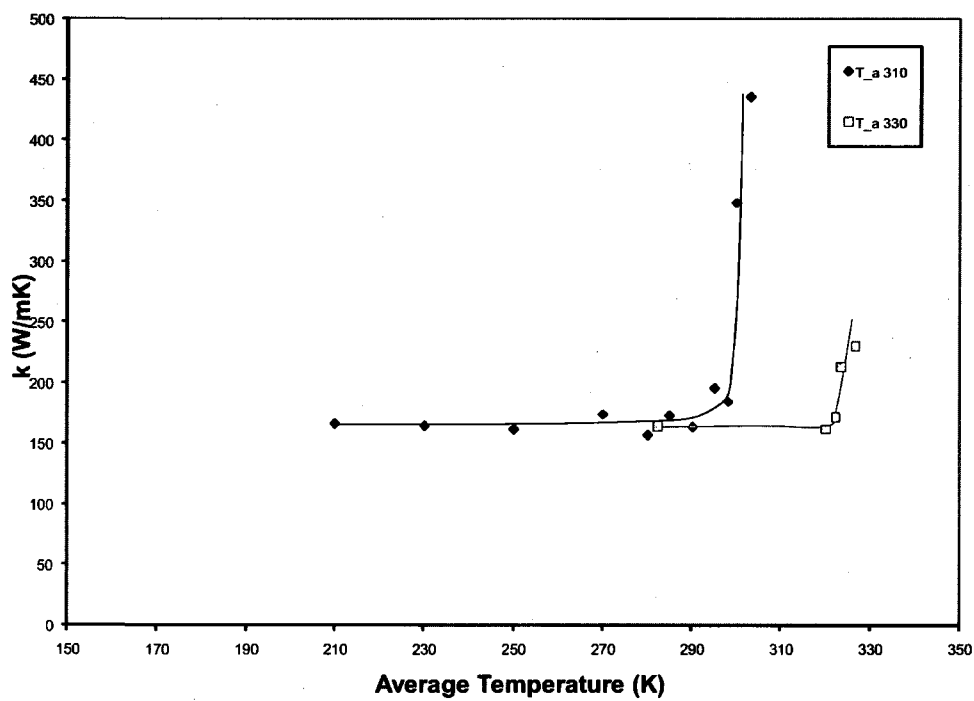


Figure 3.7 : Thermal conductivity compared for average temperature, $\frac{T_{11}+T_{12}}{2}$, of SWNT with T_a at 330K and 310K

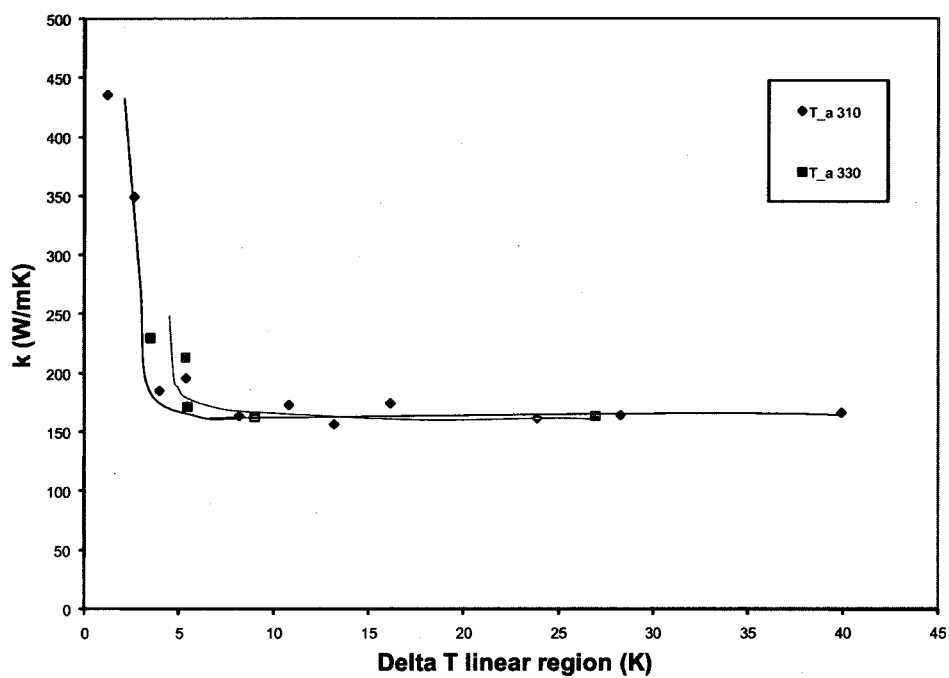


Figure 3.8 : Thermal conductivity compared change in temperature of linear part, $T_{l1} - T_{l2}$, of axial temperature profile T_a at 330K and 310K

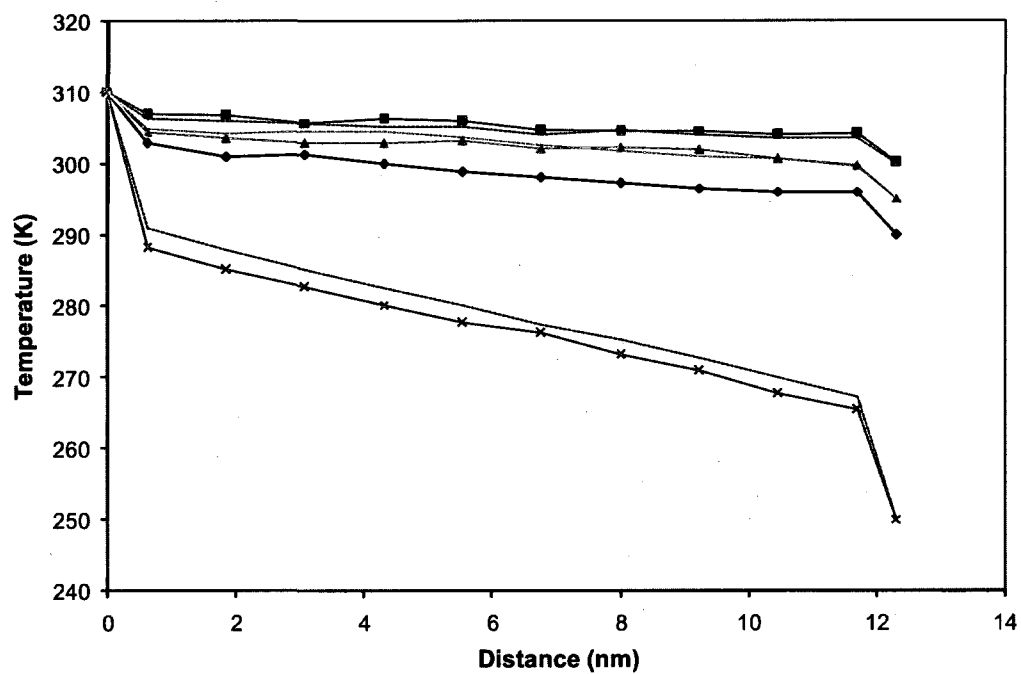


Figure 3.9 : Axial temperature profile of a SWNT (5,5) with the base temperature at 310 K at $x=0$ nm and various temperatures at $x=12.3$ nm with a heated base lengths of 24.6 nm and surrounding nitrogen at 250 K. The axial temperature profiles for a vacuum under the same conditions are plotted with the dotted line with out markers.

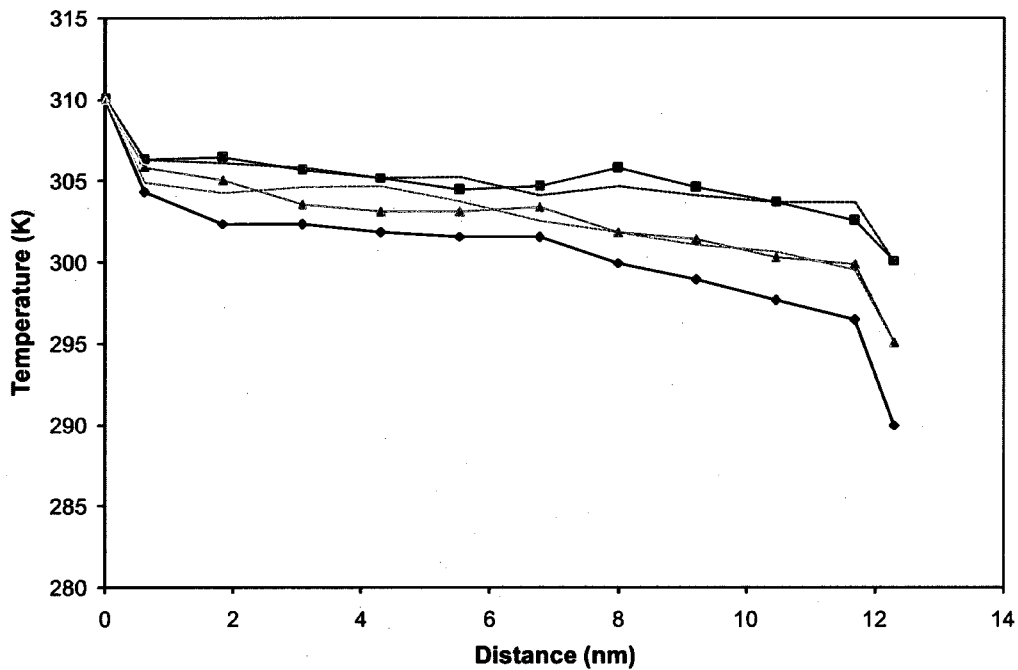


Figure 3.10 : Axial temperature profile of a SWNT (5,5) with the base temperature at 310 K at $x=0$ nm and various temperatures at $x=12.3$ nm with a heated base lengths of 24.6 nm and surrounding fluid at 290 K. The axial temperature profiles for a vacuum under the same conditions are plotted with the dotted line with out markers.

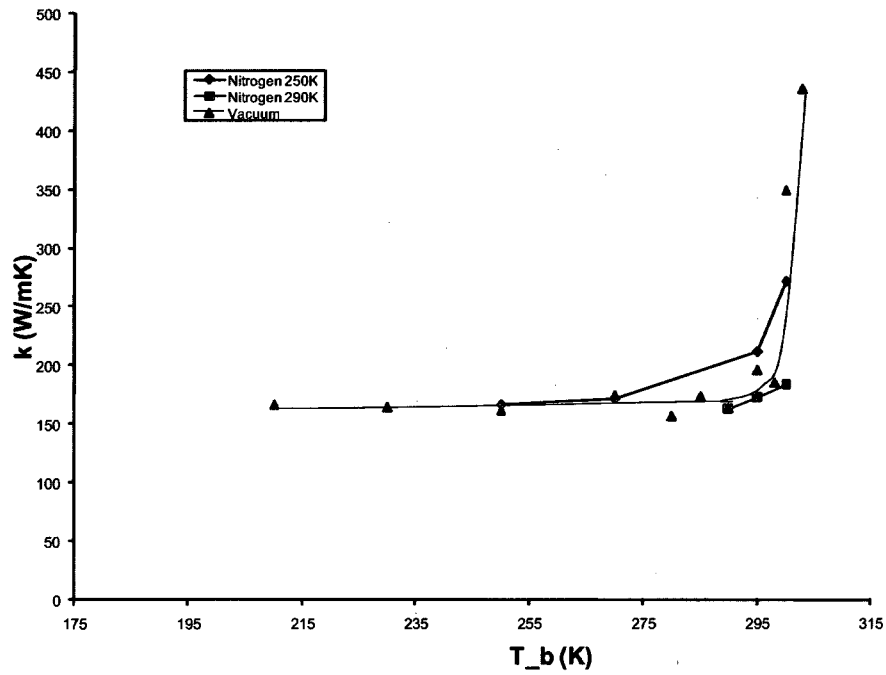


Figure 3.11 : Effective thermal conductivity compared with $T_a = 310K$ and T_b varies with nitrogen at 250K and 290K overlaid with results for thermal conductivity in a vacuum.

thermal conductivity is similar to the thermal conductivity in a vacuum with large temperature differences between T_a and T_b . As the temperature difference becomes smaller thermal conductivity appears to take a more gradual transition in nitrogen than only in a vacuum as seen in Figure 3.11. This is easily seen with the data points for when the nitrogen thermostat is set at 250K. Data points were only taken when radial heat transfer would be transferring away from the SWNT in order to make comparable data.

Effective thermal conductivity for nitrogen at 290K was relatively flat even at small temperature difference for the bases compared to the same boundary conditions in a vacuum. When the fluid temperature is 290K the effective thermal conductivity is less than in a vacuum, while an increase is shown when the fluid temperature is 250K. When nitrogen was set at 250K the thermal conductivity did not decay as steeply and had about $7W/mK$ increase in effective thermal conductivity when the base temperature difference was greater than 40K compared to same boundary conditions in a vacuum.

Chapter 4

Conclusion

A non equilibrium molecular dynamics simulation was used to determine varying thermal conductivity values in a vacuum and in nitrogen at $250K$ and $290K$. Using the output of the thermostats set to hold the end temperatures the heat flux across the SWNT was calculated. Then the temperature gradient was calculated by using time averaged sections along the SWNT. Fourier's Law was then used to calculate the thermal conductivity. The results were found to be in agreement with Maruyama. The heat flux and temperature gradient were kept as a constant by determining the length of the heated ends for convergence. It was determined that twice the length of the analyzed section was acceptable. When the high base temperature was $330K$ and $310K$ the thermal conductivities curves matches up well for similar changes in temperature of T_{l1} and T_{l2} . They had similar thermal conductivity values for temperature differences greater than $20K$ with a steep increase when the temperature differences were less than $10K$.

Preliminary results for effective thermal conductivity for a fluid showed the thermal conductivity is not the same as in a vacuum. Ballistic heat transfer should result in no radial heat transfer to the surrounding fluid; therefore, the fluid temperature and fluid itself should not effect the effective thermal conductivity. The data from the above simulations shows the surrounding fluid and temperature of the fluid has an effect on the effective thermal conductivity. The fluid may be interacting with the SWNT and transferring some thermal energy.

Future work could investigate if a radial temperature profile is developing indicating radial heat transfer. This could be accomplished by calculating the fluid temperature of the volume concentric tubes of small thickness. The concentric tubes would have to be divided up into discrete lengths because a temperature gradient exists along the length of the tube due to the heat flux. Instantaneous temperature profiles would require basic code implementation using the output in GROMACS. A time average profile, that reduces noise of output data, would be more difficult to create since a time averaged output of velocities for each atom is not created in the output file.

Bibliography

- [1] <http://en.wikipedia.org/wiki/Image:CNTnames.png>.
- [2] J. T. Frey and D. J. Doren, "Tubegen computer code," *University of Delaware, Newark, NJ*, <http://turin.nss.udel.edu/research/tubegenonline.html>, 2005.
- [3] S. Iijima, "Helical microtubules of graphitic carbon," *Nature*, vol. 354, pp. 56–58, 1991.
- [4] R. H. Baughman, A. A. Zakhidov, and W. A. de Heer, "Carbon Nanotubes—the Route Toward Applications," *Science*, vol. 297, no. 5582, pp. 787–792, 2002.
- [5] M. B. Nardelli, B. I. Yakobson, and J. Bernholc, "Brittle and ductile behavior in carbon nanotubes," *Phys. Rev. Lett.*, vol. 81, pp. 4656–4659, Nov 1998.
- [6] M. Hu, S. Shenogin, P. Keblinski, and N. Rarvika, "Air flow through carbon nanotube arrays," *Applied Physics Letters*, vol. 91, 2007.
- [7] D. Tuckermann and R. Pease, "High-performance heat sinking for vlsi," *IEEE Electron Device Lett.*, vol. EDL-2, pp. 126–129, May 1981.
- [8] "Emerging research devices." International Technology Roadmap for Semiconductors 2004 http://www.itrs.net/Links/2004Update/2004.05_ERD.pdf.
- [9] R. Prasher, J. Chang, I. Sauciuc, S. Narasimhan, G. C. D. Chau, A. Myers, S. Prstic, and C. Hu, "Nano and micro technology-based next-generation

- package-level cooling solutions,” *Intel Technology Journal*, vol. 9, no. 4, pp. 285–296, 2005.
- [10] S. Berber, Y.-K. Kwon, and D. Tománek, “Unusually high thermal conductivity of carbon nanotubes,” *Phys. Rev. Lett.*, vol. 84, pp. 4613–4616, May 2000.
- [11] L. S. P. Kim, A. Majumdar, and P. McEuen, “Thermal transport measurement of individual multiwalled nanotubes,” *Physical Review Letters*, vol. 87, no. 21, 2001.
- [12] C. Yu, L. Shi, Z. Yao, D. Li, and A. Majumdar, “Thermal conductance and thermopower of an individual single-wall carbon nanotube,” *Nano Letters*, vol. 5, no. 9, pp. 1842–1846, 2005.
- [13] K. Kordas, G. Toth, P. Moilanen, M. Kumpumaki, J. Vahakangas, A. Uusimaki, R. Vajtai, and P. Ajayan, “Chip cooling with integrated carbon nanotube microfin architectures,” *Applied Physics Letters*, vol. 90, 2007.
- [14] W. J. Mikowycz and E. M. Sparrow, eds., *Advances in Numerical Heat Transfer*, vol. 2. Taylor & Francis, 2000.
- [15] M. Hu, S. Shenogin, P. Keblinski, and N. Rarvikar, “Thermal energy exchange between carbon nanotube and air,” *Applied Physics Letters*, vol. 90, 2007.
- [16] S. Shenogin, L. Xue, R. Ozisik, P. Keblinski, and D. Cahill, “Role of thermal boundary resistance on the heat flow in carbon-nanotube composites,” *Journal of Applied Physics*, vol. 95, no. 12, 2004.
- [17] S. Huxtable, D. Cahill, S. Shenogin, L. Xue, R. Ozisik, P. Barone, M. Usrey, M. Strano, G. Siddons, M. Shim, and P. Keblinski, “Interfacial heat flow in

- carbon nanotube suspensions," *Nature Materials*, vol. 2, pp. 731–734, 2003.
- [18] M. Biercuk, M. Llaguno, M. Radosavljevic, J. Hyun, A. Johnson, and J. Fischer, "Carbon nanotubes composites for thermal management," *Applied Physics Letters*, vol. 80, no. 15, pp. 2767–2769, 2002.
- [19] M. Osman and D. Srivastava, "Temperature dependence of the thermal conductivity of single-wall carbon nanotubes," *Nanotechnology*, vol. 12, pp. 21–24, 2001.
- [20] H. Rafii-Tabar, "Computational modelling of thermo-mechanical and transport properties of carbon nanotubes," *Physics Reports*, vol. 390, pp. 235–452, 2004.
- [21] C. Huang, K. Nandakumar, P. Choi, and L. Kostiuk, "Molecular dynamics simulation of a pressure-driven liquid transport process in cylindrical nanopore using two self-adjusting plates," *J. Chem. Phys.*, vol. 124, 2006.
- [22] R. Delgado-Buscalioni, "Cyclic motion of a grafted polymer under shear flow," *Physical Review Letters*, vol. 124.
- [23] P. Padilla and S. Toxvaerd, "Simulating shear flow," *J. Chem. Phys.*, vol. 104, no. 15, pp. 2589–2596, 1996.
- [24] E. Lindahl, B. Hess, and D. Van der Spoel *J. Mol. Mod.*, vol. 7, pp. 306–317, 2001.
- [25] D. C. Rapaport, *The Art of Molecular Dynamics Simulation*. Cambridge University Press, 2004.
- [26] L. Verlet, "Computer "experiments" on classical fluids. i. thermodynamical properties of lennard-jones molecules," *Phys. Rev.*, vol. 159, p. 98, Jul 1967.

- [27] H. Berendsen, J. Postma, W. van Gunsteren, and A. DiNola *J. Chem Phys.*, vol. 81, no. 8, 1984.
- [28] J. Shiomi and S. Maruyama, "Molecular dynamics simulations of diffusive-ballistic heat conduction in carbon nanotubes," *Mater. Res. Soc. Symp. Proc.*, vol. 1002, 2007.
- [29] Y. Wu, C. H. Liu, H. Huang, and S. S. Fan, "Effects of surface metal layer on the thermal contact resistance of carbon nanotube arrays," *Applied Physics Letters*, vol. 87, no. 21, p. 213108, 2005.
- [30] Y. Guo, N. Karasawa, and W. Goddard, "Prediction of fullerene packing in c_{60} and c_{70} crystals," *Nature*, vol. 351, no. 21, pp. 464–467, 1991.
- [31] V. Cervellera, M. Alberti, and F. Huarte-Larranaga, "A molecular dynamics simulation of air adsorption in single-walled carbon nanotube bundles," *Int. J. of Quantum Chemistry*, vol. 108, pp. 1714–1720, January 2008.
- [32] S. Nose, "A molecular dynamics method for simulations in the canonical ensemble," *Mol. Phys.*, vol. 52, pp. 255–268, 1984.
- [33] W. Hoover, "Canonical dynamics: equilibrium phase-space distributions," *Phys. Rev. A*, vol. 31, pp. 1695–1697, 1985.
- [34] J. Shiomi and S. Maruyama *Japanese Journal of Applied Physics*, vol. 47, no. 4, pp. 2005–2009, 2008.
- [35] Z. Yao, J. Wang, B. Li, and G. Liu, "Thermal conduction of carbon nanotubes using molecular dynamics," *Physical Review B*, vol. 71, no. 085417, 2005.